A Quantum Chemical Study of the Atomic Layer Deposition of Al_2O_3 Using $AlCl_3$ and H_2O as Precursors

Annica Heyman[†] and Charles B. Musgrave*[,‡,§]

Departments of Applied Physics, Chemical Engineering, and Materials Science and Engineering, Stanford University, Stanford, California 94305-5025

Received: January 16, 2004; In Final Form: February 26, 2004

Atomic layer deposition (ALD) of alumina (Al_2O_3) using water and aluminum trichloride ($AlCl_3$) is studied using density functional theory (DFT). The atomistic mechanisms of the two deposition half-cycles on Al_2O_3−OH* and Al_2O_3−Cl* surface sites include the formation of stable intermediates and result in high barriers for HCl formation. Increasing the temperature reduces the stability of the intermediates but also increases the desorption rate of adsorbed precursors. Both half-reactions are qualitatively similar to the corresponding reactions of ALD of HfO_2 and ZrO_2 from H_2O and $HfCl_4$ and $ZrCl_4$, respectively, but differ significantly from the reactions of ALD of Al_2O_3 from $Al(CH_3)_3$ and H_2O. Although the high electronegativity of Cl increases the stability of the dative-bonded trapped intermediates in the Zr and Hf chloride cases, the inductive effect is stronger for $AlCl_3$, increasing the stability of adsorbed $AlCl_3$ by 29 kcal/mol relative to the adsorption energy of $Al(CH_3)_3$. Furthermore, the ligand-exchange barrier is 26 kcal/mol higher for $AlCl_3$ than for $Al(CH_3)_3$, thus reducing the reaction kinetics and increasing the ALD temperature for the $AlCl_3/H_2O$ system. We have also found a new reaction pathway which involves ligand-exchange without metal deposition which we call nongrowth ligand-exchange. This pathway is more competitive in ALD using $AlCl_3$ as the metal precursor than when using $Al(CH_3)_3$ and reduces the ALD growth rate. These results provide additional physical insight into the nature of these reaction mechanisms and demonstrate that the Cl ligands have a larger impact on the reaction energetics than the metal atom for the ALD of these high-κ oxides.

Introduction

Atomic layer deposition (ALD) is a deposition technique based on alternating self-terminating surface reactions.[1] Although it is similar to chemical vapor deposition (CVD), the self-terminating nature of the surface reactions leads to self-limiting growth unlike CVD, which is a continuous deposition process. Atomic level control in ALD film growth is achieved through a sequence of chemical reactions in which the saturating surface reactions ideally limit the growth in each cycle to one monolayer. However, because full monolayer growth per cycle is usually not achieved, deposition effects such as steric repulsion of adsorbates, desorption of adsorbed precursors, slow kinetics of the surface reactions, low surface active site density, and difficulty in removing and readsorption of reaction byproducts have been suggested as possible explanations. To determine the cause of the submonolayer growth per cycle in ALD, a detailed understanding of the surface reactions is required.

Recently, ALD has received much attention as a promising deposition technique for gate oxides in metal-oxide semiconductor field-effect transistors (MOSFET) because exceptionally uniform and conformal ultrathin films with a precisely controlled thickness can be obtained.[2] The continuing miniaturization of MOS devices is currently motivating a vigorous search for high-κ materials to replace SiO_2 as the gate oxide. As the device dimensions shrink, an increased gate capacitance is needed to ensure correct operation of the transistor. This can be achieved by decreasing the thickness of the gate dielectric, but for sub-15 Å SiO_2 gate oxides, direct tunneling of electrons through the oxide becomes substantial. Alternatively, if a higher dielectric constant material, for example Al_2O_3, HfO_2, or ZrO_2, is used as the gate dielectric, the necessary capacitance can be achieved with a physically thicker film, therefore avoiding the tunneling problem.[3]

In this work we use density functional theory (DFT) to investigate an atomistic ALD mechanism for Al_2O_3 using $AlCl_3$ and H_2O as precursors. Growing Al_2O_3 thin films from $AlCl_3$ and H_2O was among the first successful ALD processes[4,5] and has been used in industry from the very beginning of the manufacturing of thin film electroluminescent (TFEL) displays.[1] More recently Al_2O_3 has been proposed as a possible high-κ material for gate stacks in MOS devices due to its relatively high dielectric constant ($\kappa \sim 9$) compared to SiO_2 ($\kappa \sim 3.9$) but otherwise similar characteristics to those of SiO_2, such as large band gap and band-offsets and an amorphous structure at high temperatures.[6] Unfortunately, MOSFET structures fabricated with Al_2O_3 as the gate dielectric have exhibited low channel mobilities, possibly due to a large number of trapped charges in the dielectric.[3] Furthermore, aluminum oxide thin films are applicable as corrosion and wear protective coatings,[7,8] capacitance dielectrics in DRAM's,[9] and optical multilayer coatings.[10]

Experimental data on the ALD of Al_2O_3 from $AlCl_3$ and H_2O have shown that as the growth temperature increases, the refractive index of the film also increases[11] implying that the chloride and hydroxyl impurity concentrations decrease.[12]

* Corresponding author: Phone: (650) 725-9176. Fax: (650) 725-7294. E-mail: chasm@stanford.edu.
[†] Department of Applied Physics.
[‡] Department of Chemical Engineering.
[§] Department of Materials Science and Engineering.

10.1021/jp049762x CCC: $27.50
Published on Web 04/14/2004

Unfortunately, with increasing temperature, a decreasing growth rate per cycle is observed.[11] On the other hand, Al_2O_3 ALD employing trimethylaluminum [$Al(CH_3)_3$] (TMA) and water results in higher growth rates at lower temperatures compared to the metal-chloride process investigated in this work. Moreover, the films produced by Al_2O_3 ALD with TMA have a higher refractive index, despite higher levels of carbon and hydrogen contamination.[13] A theoretical study of a reaction mechanism for the Al_2O_3 ALD process with TMA and water has already been conducted.[14] We are interested in comparing the two Al_2O_3 ALD processes to investigate how a change of the ligands of the aluminum precursor affects the reaction mechanisms and kinetics. Moreover, in order to explore the general characteristics of metal-chloride precursors in ALD of high-κ oxides, we compare the two Al_2O_3 ALD processes with earlier calculations of ALD of HfO_2[15] and ZrO_2[16] from H_2O, and $HfCl_4$ and $ZrCl_4$, respectively.

Computational Details

For Al_2O_3 deposition using $AlCl_3$ and H_2O the overall reaction between the precursors and the growing surface can be separated into the two half-reactions

$$Al_2O_3{-}OH^* + AlCl_3(g) \rightarrow Al_2O_3{-}O{-}Al{-}Cl^* + HCl(g) \quad \text{(a)}$$

$$Al_2O_3{-}Cl^* + H_2O(g) \rightarrow Al_2O_3{-}OH^* + HCl(g) \quad \text{(b)}$$

where the asterisks denote surface species, which may have additional −Cl and −OH groups attached to the aluminum atom. We used the $Al(OH)_2{-}OH$, $Al(OH){-}Cl_2$, and $Al(OH)_2{-}Cl$ clusters to represent the Al−OH* and Al−Cl* surface sites. We have also used larger clusters, $Al[OAl(OH)_2]_2{-}OH$, $Al[OAl(OH)_2]{-}Cl_2$, and $Al[OAl(OH)_2]_2{-}Cl$, in order to investigate cluster truncation effects. The larger clusters include additional material neighboring the reactive site on the Al_2O_3 surface and better mimic the effects of the surrounding material. Thus, using two cluster sizes allowed us to study the effects of nearby atoms on the reaction energies. All clusters were fully relaxed, and as a result, they may underestimate the strain energy of the system. However, unrealistic distortions of the surface clusters were not observed. All clusters used are shown in Figure 1.

The detailed atomistic reaction mechanisms of (a) and (b) above, along with the associated thermochemistry, were investigated using the B3LYP[17] gradient-corrected hybrid DFT method. The wave function was expanded with the 6-31+G(d,p) double-ζ basis set with diffuse functions on heavy atoms and polarization functions on all atoms. The geometries were optimized by minimizing the energy to stationary points on the potential energy surface (PES). Frequency calculations were done to verify the nature of these stationary points and to determine the zero-point energies and thermal corrections at finite temperatures. For all transition states, intrinsic reaction coordinate (IRC) calculations were preformed to verify that the transition state connected the desired stable structures. All calculations were performed using Gaussian 98.[18]

Results

First Half-Reaction. The reaction energetics at 0 K along with the Gibbs free energies at 298 and 773 K for the first half-reaction (a) are shown in Figure 2 with the corresponding values given in Table 1. As illustrated by the 0 K PES, $AlCl_3(g)$ first adsorbs molecularly on an Al−OH* surface site. This reaction step is exothermic with an adsorption energy of −43 kcal/mol, and the Gibbs free energies are also negative with respect to the $AlCl_3(g)$ and Al−OH* reactants at the temperatures investigated. In this adsorbed state, the reactive oxygen atom of the hydroxyl surface site donates its electron lone-pair into the empty p-orbital of the aluminum atom of the adsorbing $AlCl_3(g)$ to form a dative bond. As this Al−O dative bond forms it mixes with the Al−O covalent bond between the active oxygen of Al−OH* and the surface aluminum atom to create two similar Al−O bonds of mixed dative−covalent character. In addition to the Al−O bond between $AlCl_3(a)$ and the surface −OH group, one of the chlorine atoms of $AlCl_3(a)$ forms a weak ionic bond to the aluminum atom of the surface Al−OH* site. This interaction lengthens the $Cl{-}AlCl_2$ bond involving the Cl atom coordinated to the surface to 2.27 Å from 2.10 Å in the gas-phase and from the 2.11 Å bond length for the two other Al−Cl bonds in $Cl{-}AlCl_2$, as shown in Figure 3.

The next step involves recombination of the hydrogen atom from the Al−OH* surface site with one of the chlorine atoms

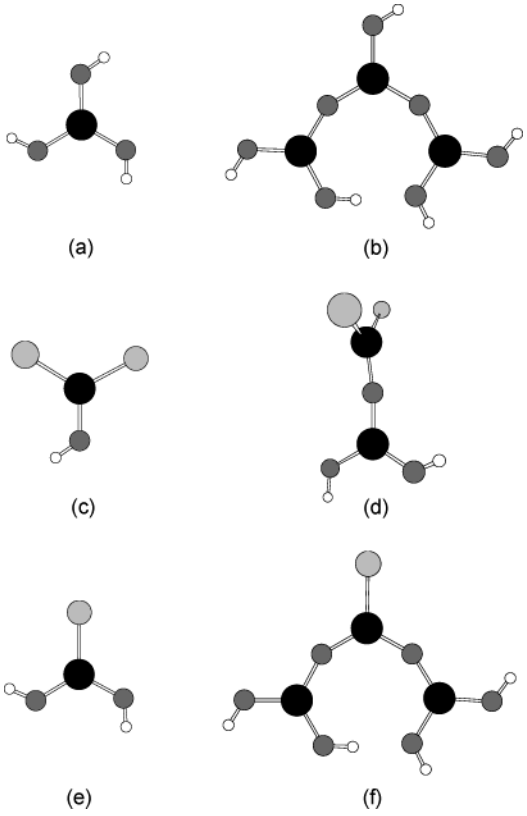

Figure 1. Cluster models used in the calculations. (a) $Al(OH)_2{-}OH$ and (b) $Al[OAl(OH)_2]_2{-}OH$ clusters representing Al−OH* surface sites. (c) $Al(OH){-}Cl_2$ and (d) $Al[OAl(OH)_2]{-}Cl_2$ clusters representing $Al{-}Cl_2$* surface sites. (e) $Al(OH)_2{-}Cl$ and (f) $Al[OAl(OH)_2]_2{-}Cl$ clusters representing Al−Cl* surface sites. Black circles denote Al, dark gray circles denote oxygen, light gray circles denote chlorine, and white circles denote hydrogen.

TABLE 1: Reaction Energies Relative to the Reactants at 0 K (ΔH_0) and Gibbs Free Energies (ΔG) at 298 K and 773 K for the $Al_2O_3{-}OH^* + AlCl_3(g)$ Half-Reaction Calculated Using the $Al[OAl(OH)_2]_2{-}OH$ Cluster[a]

	$AlCl_3$(a) complex	first TS	first HCl(a) complex	second TS	second HCl(a) complex	HCl desorption
$Al[OAl(OH)_2]_2{-}OH + AlCl_3 \rightarrow Al[OAl(OH)_2]_2{-}O{-}AlCl_2 + HCl$						
ΔH_0	−43	−6.8	−6.8	−5.3	−5.7	−3.8
ΔG_{298}	−30	4.8	3.7	5.4	3.0	−2.1
ΔG_{773}	−11	23	18	22	15	−1.3

[a] All energies are shown in kcal/mol.

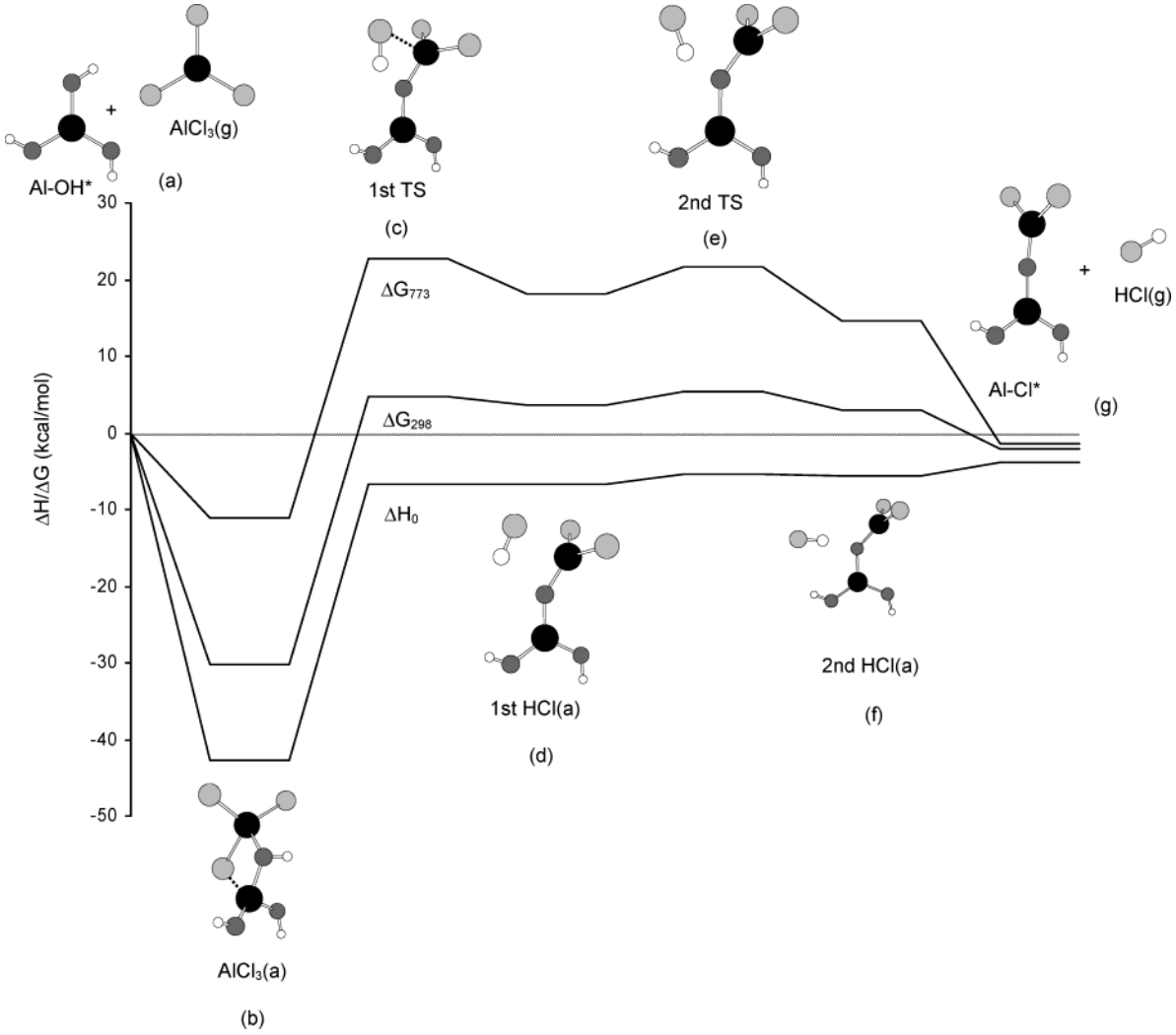

Figure 2. Potential energy surface (ΔH_0) and Gibbs free energy surfaces at 298 K (ΔG_{298}) and 773 K (ΔG_{773}) for the Al[OAl(OH)$_2$]$_2$−OH + $AlCl_3$ reaction, representing the first half-reaction. The structures are shown using the Al(OH)$_2$−OH cluster for clarity. The stationary points correspond to (a) Al−OH* + $AlCl_3$(g) reactants, (b) the $AlCl_3$(a) complex, (c) the first HCl(a) formation transition state with transfer of hydrogen from oxygen to chlorine, (d) the first HCl(a) physisorbed state, (e) the second HCl(a) transition state dissociating the Al−Cl bond, (f) the second HCl(a) physisorbed state, and (g) the Al−Cl* + HCl(g) products.

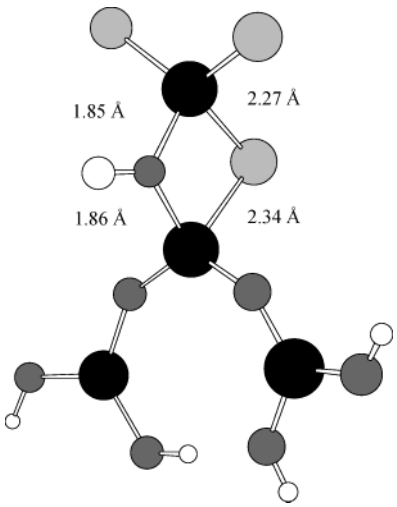

Figure 3. The $AlCl_3$(a) complex formed in the first half-reaction. The bond lengths displayed should be compared to the 1.70 Å Al−O bond in Al(OH)$_3$ and the 2.10 Å Al−Cl bond in $AlCl_3$.

of $AlCl_3$(a), resulting in physisorbed HCl(a) on the surface. This step is, however, divided into two energetically similar steps. In the first step, corresponding to the first transition state in Figure 2, the hydrogen transfers from the surface hydroxyl group to one of the chlorine atoms of $AlCl_3$(a). The second step involves the dissociation of the Al−Cl bond and proceeds through the second transition state shown in Figure 2. The formation of HCl(a) is activated with respect to the chemisorbed $AlCl_3$(a) state with activation energies of 36 and 37 kcal/mol for the two HCl(a) states in Figure 2, respectively. Because the adsorbed complex and the transition states are entropically similar in that they involve no gas-phase species, the activation free energies of the two transition states with respect to the $AlCl_3$(a) adsorbed state are nearly independent of temperature. Furthermore, their entropies are much lower than those of the initial and final states of the half-reaction which involve the gas-phase precursor and byproducts, respectively. Therefore, as the temperature increases, the Gibbs free energies of states with gas-phase species are stabilized relative to the adsorbed states and transition states.

To ensure that the two transition states are not artifacts of the choice of method or basis set, we performed more extensive calculations on this half-reaction. First, we extended the basis set and repeated the transition state calculations using the B3LYP/6-311++G(d,p) level of theory. Next, we performed transition state searches using the original basis set and Møller−

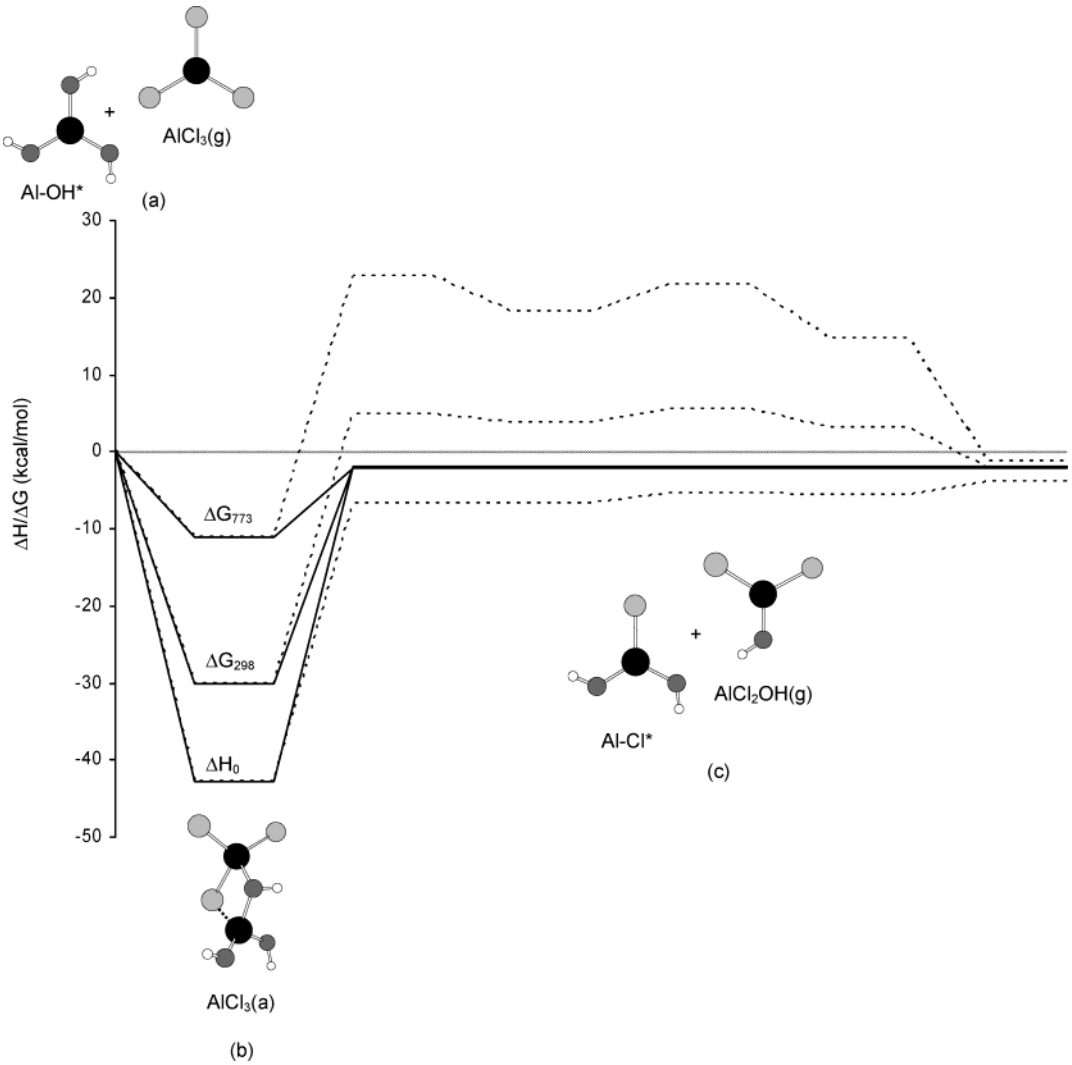

Figure 4. Potential energy surfaces (ΔH_0) and Gibbs free energy surfaces at 298 K (ΔG_{298}) and 773 K (ΔG_{773}) for the nongrowth ligand-exchange reaction (solid) and, as comparison, the first half-reaction (dashed). The structures are shown using the $Al(OH)_2-OH$ cluster for clarity. The stationary points correspond to (a) Al−OH* + $AlCl_3$(g) reactants, (b) the $AlCl_3$(a) complex, and (c) the Al−Cl* + $AlCl_2OH$ dissociated products.

Plesset second-order perturbation theory (MP2) followed by single-point energies calculated using quadratic configuration interaction including single and double excitations and triples corrections (QCISD(T)) at the MP2 geometries. Both approaches resulted in the same transition states as found using B3LYP with the original basis set with differences in relative energies that were less than 3 kcal/mol.

The product of this half-reaction is HCl which is physisorbed onto the surface. However, the desorption energy is only 2 kcal/mol for the final HCl(a) state, and at 298 K the Gibbs free energy of the physisorbed HCl(a) state is higher than the desorbed product. The first half-reaction results in the conversion of the −OH terminated surface to a −Cl terminated surface with the addition of up to a monolayer of Al atoms to the film.

Nongrowth Ligand-Exchange Reaction. Figure 3 suggests the possibility of an additional reaction pathway from the $AlCl_3$(a) state. One chlorine atom of $AlCl_3$(a) is weakly bound to the Al atom of the Al−OH* surface site. This Cl atom can transfer to the surface aluminum atom by forming a covalent bond to the surface Al and breaking its bond to the aluminum atom of $AlCl_3$(a) while the surface hydroxyl of Al−OH* simultaneously breaks its mixed dative−covalent Al−O bond with the surface Al, converting its mixed covalent−dative bond to the Al atom of $AlCl_3$(a) to a covalent bond. The products are an $AlCl_2OH$(g) molecule and a −Cl terminated surface site, Al−Cl*, which is the same surface termination created by the ligand-exchange mechanism of the first half-reaction. However, this alternative mechanism, which we call "nongrowth ligand-exchange", does not lead to the deposition of an aluminum layer, and consequently, this competing reaction does not contribute to film growth. Furthermore, the −Cl termination that results from nongrowth ligand-exchange blocks further reaction with the metal precursor in the same way −Cl termination limits growth to no more than one monolayer per half-cycle.

The energetics for the nongrowth ligand-exchange reaction are shown in Figure 4, where for comparison the corresponding energies for the first half-reaction are shown with dashed lines. The energetics of the nongrowth reaction are summarized in Table 2. We found no transition state for the nongrowth ligand-exchange mechanism, and consequently, its activation barrier is the reaction energy. The products of the nongrowth ligand-exchange reaction are located at −2 kcal/mol with respect to the reactants at 0 K. The near thermal neutrality of the reaction is expected because the nongrowth ligand-exchange reactions using any ALD precursor are isodesmic because the reaction conserves the number and types of bonds. As illustrated in Figure 4, the nongrowth reaction can kinetically compete with the first ALD half-reaction, especially at the high temperatures required for the $AlCl_3$/water process, because the activation barriers for these two reactions differ by only 3 kcal/mol.

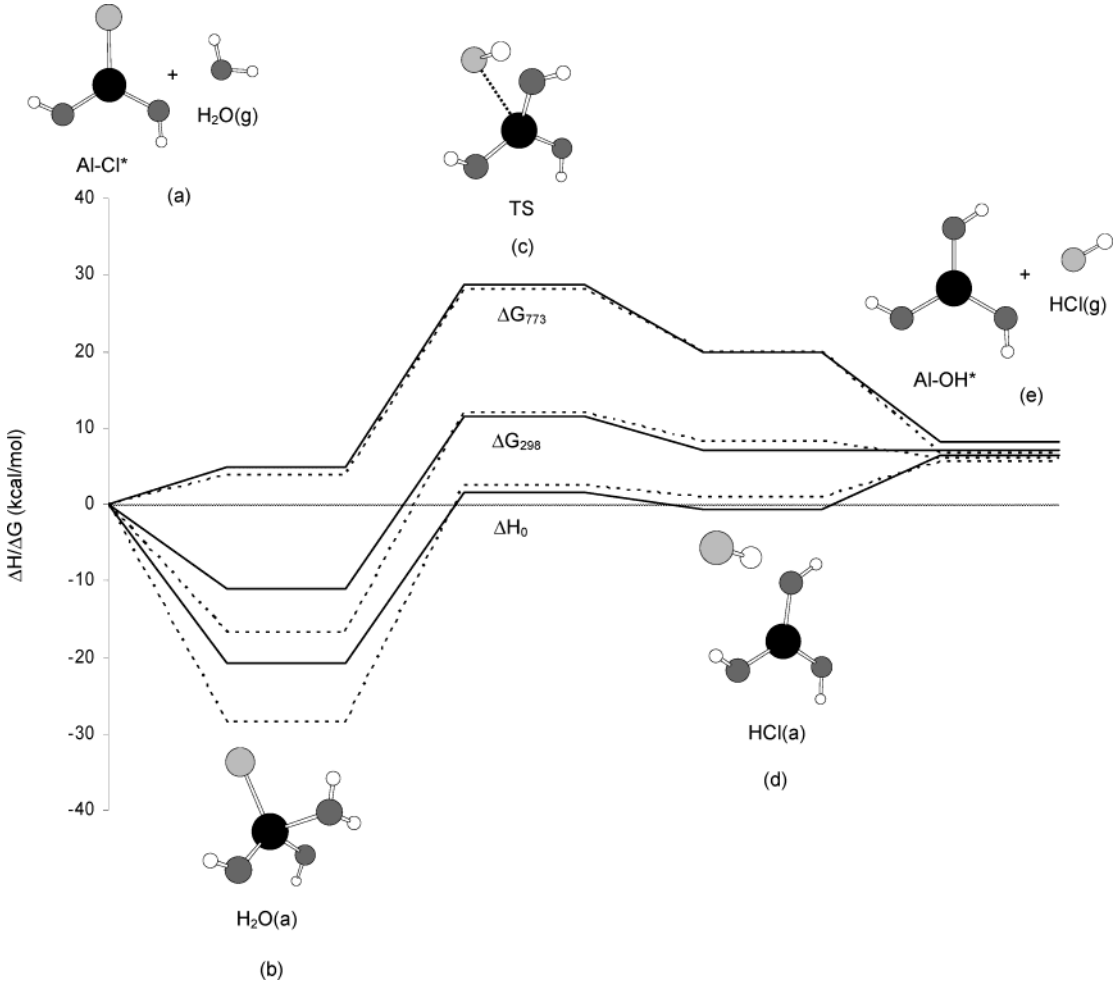

Figure 5. Potential energy surfaces (ΔH_0) and Gibbs free energy surfaces at 298 K (ΔG_{298}) and 773 K (ΔG_{773}) for the Al[OAl(OH)$_2$]$-$Cl$_2$ + H$_2$O reaction (dashed) and the Al[OAl(OH)$_2$]$_2-$Cl + H$_2$O reaction (solid), representing the two reactions of the second half-reaction. The structures shown are for the Al[OAl(OH)$_2$]$_2-$Cl + H$_2$O reaction using only the Al(OH)$_2-$Cl cluster for clarity. The stationary points correspond to (a) the Al$-$Cl* + H$_2$O(g) reactants, (b) the H$_2$O(a) complex, (c) the HCl(a) formation transition state, (d) the HCl(a) physisorbed state, and (e) the Al$-$OH* + HCl(g) dissociated products.

TABLE 2: Reaction Energies Relative to the Reactants at 0 K (ΔH_0) and Gibbs Free Energies (ΔG) at 298 K and 773 K for the Nongrowth Ligand-Exchange Reaction Using the Al[OAl(OH)$_2$]$_2-$OH Cluster[a]

	H$_2$O(a) complex	AlCl$_2$OH desorption
Al[OAl(OH)$_2$]$_2-$OH + AlCl$_3$ → Al[OAl(OH)$_2$]$_2-$Cl + AlCl$_2$OH		
ΔH_0	−43	−2.0
ΔG_{298}	−30	−2.0
ΔG_{773}	−11	−2.1

[a] All energies are shown in kcal/mol.

Consequently, the nongrowth ligand-exchange reaction can reduce the overall ALD growth rate.

We have found similar nongrowth ligand-exchange reactions for HfO$_2$ ALD using hafnium alkylamides,[19] alkoxides, and HfCl$_4$.[20] Similar to what we find for ALD of Al$_2$O$_3$ using AlCl$_3$, the nongrowth ligand-exchange reaction is kinetically competitive for ALD of HfO$_2$ using HfCl$_4$. It is also competitive in the case of hafnium alkoxide precursors because like HfCl$_4$, the ligand-exchange barrier is just below the entrance channel. On the other hand, the nongrowth ligand-exchange reaction is less competitive for HfO$_2$ ALD when using an alkylamide metal-lorganic precursor due to the lower activation barriers for alkylamide ligand-exchange reactions. In the case of ALD of Al$_2$O$_3$ using TMA and water, the ligand-exchange barrier for the first half-reaction is only 2.1 kcal/mol below the entrance channel,[14] which is expected to be similar to the near thermal neutral nongrowth reaction energy. However, because the low activation barriers for the TMA/water process enable low ALD temperatures, the ligand-exchange mechanism still dominates. Halls et al.[21] have recently suggested that when depositing TMA on H-passivated Si(100) 2 × 1 surfaces, gas-phase reactions between TMA and residual water analogous to the nongrowth ligand-exchange surface reactions we have predicted produce Al(CH$_3$)$_2$OH.

Second Half-Reaction. Addition of oxygen takes place in the second half-cycle where the Al$-$Cl* surface resulting from the first half-cycle is exposed to the oxygen source, in this case H$_2$O(g). We therefore investigated the reactions of H$_2$O(g) with Al$-$Cl* sites where the surface aluminum has either one or two chlorine atoms. The resulting changes in enthalpy at 0 K together with the Gibbs free energy surfaces at 298 and 773 K for both types of sites, Al$-$Cl$_2$* (dashed) and Al$-$Cl* (solid), are shown in Figure 5 and the corresponding energies are given in Tables 3 and 4. The two reaction pathways we have calculated are similar to the one found for the first half-cycle, however, they both have only one transition state. First, H$_2$O(g) molecularly absorbs on the Al$-$Cl* surface site with an adsorption energy of 28 kcal/mol for the Al$-$Cl$_2$* site and 21 kcal/mol for the Al$-$Cl* site. The formation of the adsorbed complex is followed by the transfer of one hydrogen atom of H$_2$O(a) to one of the

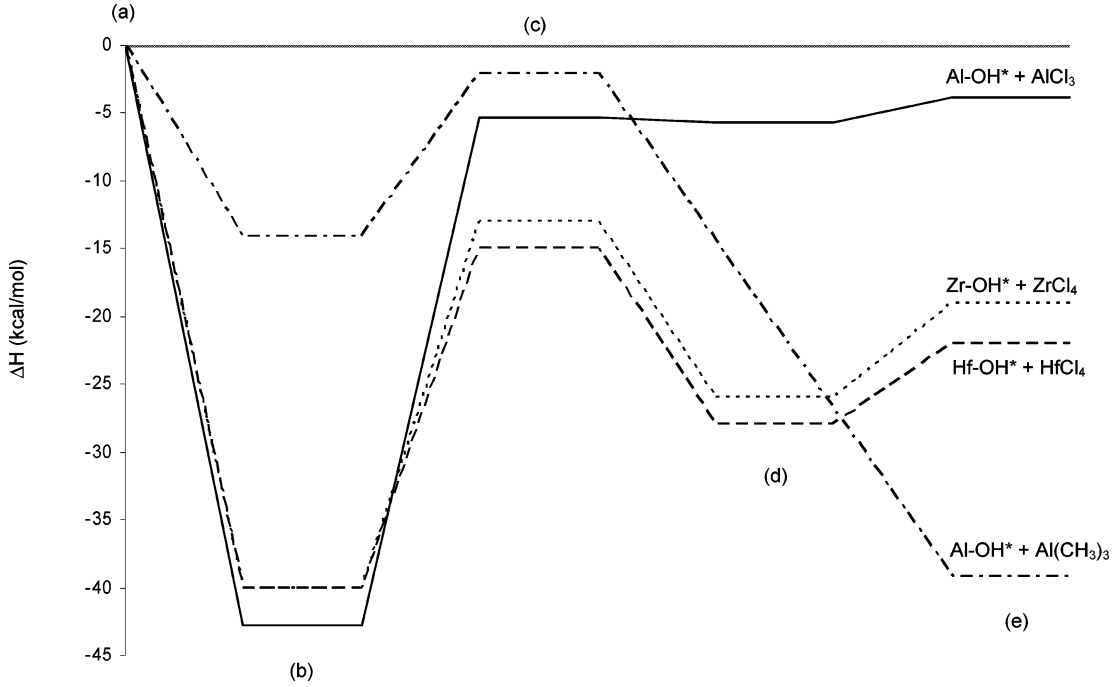

Figure 6. Reaction paths and predicted energies for the first half-reaction for four different ALD processes: Al_2O_3 from $AlCl_3$ and H_2O (solid), Al_2O_3 from TMA and H_2O (dash-dotted), HfO_2 from $HfCl_4$ and H_2O (dashed), and ZrO_2 from $ZrCl_4$ and H_2O (dotted). (a) Reactants (M−OH* and MCl_x or $Al(CH_3)_3$ depending on reaction), (b) adsorbed complex, (c) byproduct (HCl or CH_4) ligand-exchange transition state (only one transition state for the $AlCl_3$ process is displayed for clarity), (d) byproduct physisorbed state, and (e) dissociated products (M−Cl* and HCl or Al−CH_3* and CH_4).

TABLE 3: Reaction Energies Relative to the Reactants at 0 K (ΔH_0) and Gibbs Free Energies (ΔG) at 298 K and 773 K for the Al−Cl_2* + H_2O(g) Half-Reaction Calculated Using the Al[OAl(OH)$_2$]−Cl_2 Cluster[a]

	H_2O(a) complex	TS	HCl(a) complex	HCl desorption
Al[OAl(OH)$_2$]−Cl_2 + H_2O → Al[OAl(OH)$_2$]−OHCl + HCl				
ΔH_0	−28	2.5	0.82	5.6
ΔG_{298}	−17	12	8.2	6.0
ΔG_{773}	3.9	28	20	6.6

[a] All energies are shown in kcal/mol.

TABLE 4: Reaction Energies Relative to the Reactants at 0 K (ΔH_0) and Gibbs Free Energies (ΔG) at 298 K and 773 K for the Al−Cl* + H_2O(g) Half-Reaction Calculated Using the Al[OAl(OH)$_2$]$_2$−Cl Cluster[a]

	H_2O(a) complex	TS	HCl(a) complex	HCl desorption
Al[OAl(OH)$_2$]$_2$−Cl + H_2O → Al[OAl(OH)$_2$]$_2$−OH + HCl				
ΔH_0	−21	1.7	−0.67	6.4
ΔG_{298}	−11	12	7.2	7.1
ΔG_{773}	4.9	29	20	8.2

[a] All energies are shown in kcal/mol.

chlorine atoms of the Al−Cl* surface site producing physisorbed HCl(a). The formation of HCl(a) is activated with respect to the chemisorbed H_2O(a), and the HCl desorption process is endothermic. A comparison of the reaction energy diagrams for the sites with one and two Cl atoms shows that both surface sites produce similar reaction pathways and energetics with only one notable exception. In the adsorbed state on the Al−Cl_2* surface site, one of the hydrogen atoms of H_2O(a) forms a hydrogen bond with an oxygen atom in the cluster representing an oxygen atom of the Al_2O_3 surface near the reaction site. This does not happen for the reaction on the Al−Cl* site. The hydrogen bond that forms in the reaction on the Al−Cl_2* site results in an energy difference of 7 kcal/mol between the two adsorbed states on the two surface sites.

Discussion

Adsorbed Complexes. The adsorbed complexes in both half-reactions are formed by an oxygen lone-pair donation into an empty aluminum p-orbital. In the first half-reaction the lone-pair is donated by the oxygen of the Al−OH* surface site, whereas the empty p-orbital is from the aluminum atom of $AlCl_3$(g). For the second half-reaction the situation is reversed with the lone-pair instead being supplied by the oxygen of H_2O(g). All cluster models of the surface and the $AlCl_3$ precursor exhibit a planar structure implying that one Al 3s and two Al 3p orbitals hybridize to form 3 sp^2 orbitals which bond to the −OH and −Cl ligands or oxygen atoms of the surface. This leaves aluminum with one empty 3p orbital to form a dative bond by accepting an oxygen lone-pair. The same lone-pair donation has also been predicted in ALD of Al_2O_3 with TMA and H_2O.[14] A similar dative-bonded intermediate is also predicted for ALD of HfO_2[15] and ZrO_2[16] using H_2O and $HfCl_4$ or $ZrCl_4$ precursors, respectively, but where the metal atom accepts a lone-pair into an empty d-orbital. It is possible that surface Al atoms may have dative bonds to subsurface oxygen atoms, in which case the Al atom would not accept an oxygen lone-pair from water, precluding the dative-bonded intermediate H_2O(a). Such a situation should, however, not lead to significant changes in the energies of the ligand-exchange mechanisms for the first half-reaction with $AlCl_3$ since the surface Al atom is not directly involved in the ligand-exchange reaction. The situation is different in the cases of ZrO_2 and HfO_2 ALD because Zr and Hf can both have coordination numbers as high as eight, allowing them to form several dative bonds to subsurface oxygen atoms and still remain active toward forming the H_2O(a) dative-bonded complex.

Film Growth. Both the $AlCl_3$(a) and the H_2O(a) dative-bonded complexes have lower energies than the dissociated

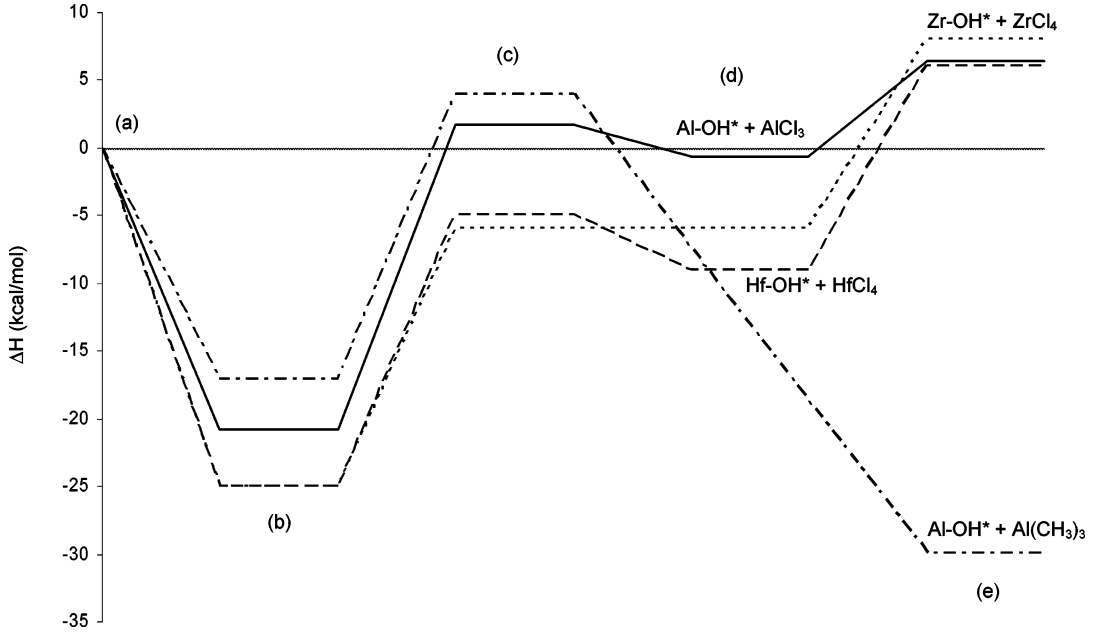

Figure 7. Reaction paths and predicted energetics for the final reaction in the second half-reaction for four different ALD processes: Al_2O_3 from $AlCl_3$ and H_2O (solid), Al_2O_3 from TMA and H_2O (dash-dotted), HfO_2 from $HfCl_4$ and H_2O (dashed), and ZrO_2 from $ZrCl_4$ and H_2O (dotted). (a) Reactants (M−Cl* or Al−CH_3* depending on reaction and H_2O), (b) adsorbed complex, (c) byproduct (HCl or CH_4) formation transition state, (d) byproduct physisorbed state, and (e) dissociated products (M−OH* and HCl or CH_4).

products. As a result, there is a high probability that, instead of direct dissociation to form the products, a significant fraction of precursor molecules will be molecularly trapped in the adsorbed complex state and the kinetics of the half-reaction will be dominated by the rate of conversion of the trapped intermediate state to the product state. The ALD process is a nonequilibrium process because the gas flow during the exposure and purge phases of the reaction cycle enables reaction byproducts to be removed from the reactor so that nonequilibrium concentrations of surface species can be obtained. However, the larger the ligand-exchange barrier relative to the adsorbed complex, the longer the nonequilibrium flow condition must be maintained to convert the adsorbed complex to the ligand-exchange products.

Because the products of the ligand-exchange mechanism are necessary to activate the surface for the following half-cycle, a trapping effect will not only lower the ligand conversion rate, but may also lower the film growth rate and result in incorporation of Cl atoms and OH groups in the film. As both Figures 2 and 5 show, higher temperatures decrease the stability of the adsorbed complexes relative to the reactants and dissociated products due to the higher entropy of the gas-phase reactants and products, thus reducing the trapping effect. This may explain the decrease in the Cl and OH concentrations in the grown film with increasing temperature that has been observed experimentally.[12] A temperature of 773 K results in only approximately 0.5% chloride incorporation in the film.[13] However, higher temperatures have been observed to decrease the film growth rate[11] instead of increasing it as the temperature dependence of converting trapped states to dissociated products suggests. Several effects may explain the lower growth rate at higher temperatures. First, the free energy of desorption of the adsorbed precursors from the trapped intermediate state decreases relative to the barrier of the ligand-exchange growth reaction with increasing temperature. This results in higher fractions of adsorbed precursor desorbing from the surface rather than dissociating to form the film and byproducts leading to longer exposure times required to reach the saturation coverage. Furthermore, the nongrowth ligand-exchange reaction becomes more kinetically competitive with increasing temperature. Another possible effect is that the surface −OH group concentration may decrease with increasing temperature due to reaction between surface hydroxyl groups to form water through a condensation reaction.[2,22] Our calculations presented here and our unpublished results for recombination of surface −OH groups indicate that it is likely that all these effects are active in ALD of Al_2O_3 using $AlCl_3$ (TCA) and water and in combination lead to lower growth rates at higher temperatures.

Cluster Size Effects. The two different clusters used in this study to represent the Al_2O_3 surface show very similar results. In terms of reaction pathways, the only discrepancy between the two cluster sizes, as described below, can be interpreted as an artifact of using the smaller cluster resulting from the smaller cluster not including direct interactions between the adsorbed precursor and neighboring surface atoms. The difference occurs for the second half-reaction on the Al−Cl* surface site. For the smaller cluster the reaction goes through two energetically similar states, corresponding to two different orientations of the adsorbed water molecule separated by a barrier of less than 2 kcal/mol. For the larger cluster, on the other hand, the water orientation enabling the ligand-exchange reaction is the most energetically favorable, and therefore, only one absorbed state occurs on the reaction pathway for the larger cluster. In terms of energies the results obtained with the larger clusters are all within 2 kcal/mol of the corresponding values of the small clusters. The only exception is the adsorbed state on the Al−Cl_2* site. As mentioned earlier, in this case a hydrogen bond is formed with an oxygen atom of the larger cluster, but because the same oxygen is not present in the smaller cluster, no bond is formed in that case. The small differences in reaction pathways and energies show that the ALD reactions of $AlCl_3$ and H_2O do not exhibit any significant nonlocal effects on the surface. Therefore, the use of cluster models should be sufficient to determine the reaction mechanisms, although care should be taken to include atoms which may directly interact with the active atoms of the reaction.

Comparisons between Different Precursors and Films. Figure 6 shows the 0 K PES for the first half-reaction of four

ALD processes: Al−OH* reacting with $AlCl_3$, Al−OH* reacting with TMA, Hf−OH* reacting with $HfCl_4$, and Zr−OH* reacting with $ZrCl_4$. As the figure illustrates, all three metal-chloride reactions are quite similar despite the differences between Al and the Zr and Hf transition metals. They all have metal half-reactions forming stable adsorption complexes, large activation energies for formation of physisorbed HCl(a), and positive HCl desorption energies. This is not the case for the Al_2O_3 metal-methyl ALD process using TMA nor for the ALD of HfO_2 and ZrO_2 using alkylamide precursors[19]. A characteristic of the adsorbed complexes in the case of metal-chlorides is that they are stabilized due to the high electronegativity of the Cl ligands which withdraw charge from the metal center thus making it a better Lewis acid. Furthermore, because there is little thermodynamic driving force for the ligand-exchange reactions in the case of metal-chloride precursors, the activation barriers relative to the adsorbed complexes for the ALD growth reactions are large and the reverse reactions from the physisorbed HCl(a) product state have low barriers, leading to a fast reverse ligand-exchange reaction at the reaction site or at a downstream site through readsorption of HCl and reverse ligand-exchange.

Among the metal-chloride processes the TCA/water process exhibits the highest activation barrier and is also the least exothermic. The $AlCl_3$(a) dative-bonded intermediate is 29 kcal/mol more stable than the TMA trapped intermediate. Furthermore, the ligand-exchange barrier is 26 kcal/mol larger than the ligand-exchange barrier for the TMA reaction. These large differences explain the higher growth temperatures required for growing Al_2O_3 using TCA than when using TMA. In fact, the more pronounced inductive effect of Cl on Al than on Zr or Hf also increases the TCA/H_2O ALD temperature relative to that of ZrO_2 and HfO_2 grown using metal-chloride precursors. The higher ALD temperature is expected to make the nongrowth ligand-exchange pathway kinetically more competitive in the case of ALD using TCA than when using TMA. Figure 7 shows a similar comparison to that shown in Figure 6, but for the second half-reaction that removes the last ligand from the surface site using water. The three potential energy surfaces of the second half-reaction of the metal-chloride ALD processes for Al_2O_3, ZrO_2, and HfO_2 are even more similar to each other than the three different PESs of the first half-reaction shown in Figure 6. The metal-chloride processes have qualitatively similar PESs and are all endothermic and have positive HCl desorption energies, two properties not exhibited by the metal-methyl process.

Conclusions

In conclusion, we have proposed a detailed atomistic reaction mechanism for Al_2O_3 ALD using $AlCl_3$ and H_2O as precursors. We have demonstrated that the inductive effects of precursor ligands can significantly change the stability of trapped intermediates and thus qualitatively alter the kinetics and thermochemistry of ALD of Al_2O_3, ZrO_2, and HfO_2 using metal precursors and water as reactants. We have presented the PES of both half-reactions along with the Gibbs free energies at 298 and 773 K, demonstrating that a high growth temperature is necessary to decrease the stability of the formed adsorption complexes but also that a high temperature makes desorption of precursors favorable, resulting in lower growth rates. Furthermore, we have investigated an alternative nongrowth ligand-exchange reaction which is kinetically competitive with the ligand-exchange mechanism. We expect that the nongrowth ligand-exchange pathway is more competitive in the TCA/water process than in the TMA/water process because, although the differences between the activation barriers for both pathways are similar for both processes, the TMA/water ALD temperature is significantly lower than that for the TCA/water process. Because this reaction deactivates a surface site, and does not deposit a metal atom, it can lead to lower growth rates. We have also compared the $AlCl_3/H_2O$ results with earlier results of ALD of Al_2O_3 from TMA and H_2O and of ALD of HfO_2 and ZrO_2 from H_2O and $HfCl_4$ and $ZrCl_4$, respectively, showing that (1) for Al_2O_3 films, a metal-chloride precursor gives a thermodynamically and kinetically less favorable process compared to the metal-methyl precursor and (2) the chlorine ligands are of more importance than the metal in determining the nature of the reaction PES. These results provide physical insight into the nature of the chemistry of ALD and demonstrate how precursor ligands can significantly alter the optimum ALD process window and characteristics.

Acknowledgment. The authors thank Joseph Han and Collin Mui for their valuable help. Support of this work from the Stanford Center for Integrated Systems (CIS) and the Initiative for Nanoscale Materials Processing, as well as the Materials Structures and Devices MARCO Center and an Office of Naval Research MURI is gratefully acknowledged.

References and Notes

(1) Ritala, M.; Leskelä, M. In *Handbook of Thin Film Materials*; Nalwa, H. S., Ed.; Academic Press: San Diego, CA, 2001; Vol. 1, Chapter 2.
(2) George, S. M.; Ott, A. W.; Klaus, J. W. *J. Phys. Chem.* **1996**, *100*, 13121.
(3) Wilk, G. D.; Wallace, R. M.; Anthony, J. M. *J. Appl. Phys.* **2001**, *89*, 5243.
(4) Suntola, T. S.; Pakkala, A. J.; Lindfors, S. G. U.S. Patent No. 4389973, 1983.
(5) Suntola, T. S.; Pakkala, A. J.; Lindfors, S. G. U.S. Patent No. 4413022, 1983.
(6) Manchanda, L.; Morris, M. D.; Green, M. L.; van Dover: R. B.; Klemens, F.; Sorsch, T. W.; Silverman, P. J.; Wilk, G.; Busch, B.; Aravamudhan, S. *Microelectron. Eng.* **2001**, *59*, 351.
(7) van Corbach, H. D.; Haanappel, V. A. C.; Fransen, T.; Gellings, P. J. *Thin Solid Films* **1994**, *239*, 31.
(8) Lux, B.; Colombier, C.; Altena, H.; Stjernberg, K. *Thin Solid Films* **1986**, *138*, 49.
(9) Yang, W. S.; Kim, Y. K.; Yang, S.-Y.; Choi, J. H.; Park, H. S.; Lee, S. I.; Yoo, J.-B. *Surf. Coat. Technol.* **2000**, *131*, 79.
(10) Riihelä, D.; Ritala, M.; Matero, R.; Leskelä, M. *Thin Solid Films* **1996**, *289*, 250.
(11) Aarik, J.; Aidla, A.; Jaek, A.; Kiisler, A. A.; Tammik, A. A. *Acta Polytech. Scand., Chem. Technol. Metall. Ser.* **1990**, *195*, 201.
(12) Hiltunen, L.; Kattelus, H.; Leskelä, M.; Makela, M.; Niinistö, L.; Nykänen, E.; Soininen, P.; Tiitta, M. *Mater. Chem. Phys.* **1991**, *28*, 379.
(13) Yun, S. J.; Lee, K.-H.; Skarp, J.; Kim, H.-R.; Nam, K.-S. *J. Vac. Sci. Technol., A* **1997**, *15*, 2993.
(14) Widjaja, Y.; Musgrave, C. B. *Appl. Phys. Lett.* **2002**, *80*, 3304.
(15) Widjaja, Y.; Musgrave, C. B. *J. Chem. Phys.* **2002**, *117*, 1931.
(16) Widjaja, Y.; Musgrave, C. B. *Appl. Phys. Lett.* **2002**, *81*, 304.
(17) Becke, A. D. *J. Chem. Phys.* **1993**, *98*, 1372.
(18) Frisch, M. J.; Trucks, G. W.; Schlegel, H. B.; Scuseria, G. E.; Robb, M. A.; Cheeseman, J. R.; Zakrzewski, V. G.; Montgomery, J. A., Jr.; Stratmann, R. E.; Burant, J. C.; Dapprich, S.; Millam, J. M.; Daniels, A. D.; Kudin, K. N.; Strain, M. C.; Farkas, O.; Tomasi, J.; Barone, V.; Cossi, M.; Cammi, R.; Mennucci, B.; Pomelli, C.; Adamo, C.; Clifford, S.; Ochterski, J.; Petersson, G. A.; Ayala, P. Y.; Cui, Q.; Morokuma, K.; Rega, N.; Salvador, P.; Dannenberg, J. J.; Malik, D. K.; Rabuck, A. D.; K., R.; Foresman, J. B.; Cioslowski, J.; Ortiz, J. V.; Baboul, A. G.; Stefanov, B. B.; Liu, G.; Liashenko, A.; Piskorz, P.; Komaromi, I.; Gomperts, R.; Martin, R. L.; Fox, D. J.; Keith, T.; Al-Laham, M. A.; Peng, C. Y.; Nanayakkara, A.; Challacombe, M.; Gill, P. M. W.; Johnson, B.; Cheng, W.; Wong, M. W.; Andres, J. L.; Gonzales, C.; Head-Gordon, M.; Replogle, E. S.; Pople, J. A. *Gaussian 98*, revision A.11.2; Gaussian, Inc.: Pittsburgh, PA, 2001.
(19) Han, J.; Wang, S.; Gordon, R. G.; Musgrave, C. B. Submitted, 2003.
(20) Mui, C.; Musgrave, C. B. Submitted, 2003.
(21) Halls, M.; Raghavachari, K.; Frank, M.; Chabal, Y. *Phys. Rev. B* **2003**, *68*, 161302.
(22) Matero, R.; Rahtu, A.; Ritala, M.; Leskelä, M.; Sajavaara, T. *Thin Solid Films* **2000**, *368*, 1.